Vehicular Motion-based DOA Estimation with a Limited Amount of Snapshots for Automotive MIMO Radar

Yuan, Sen; Fioranelli, Francesco; Yarovoy, Alexander

Important note
To cite this publication, please use the final published version (if applicable).
Please check the document version above.

Vehicular-Motion-Based DOA Estimation With a Limited Amount of Snapshots for Automotive MIMO Radar

SEN YUAN , Graduate Student Member, IEEE
FRANCESCO FIORANELLI , Senior Member, IEEE
ALEXANDER G. YAROVOY, Fellow, IEEE
Delft University of Technology, Delft, The Netherlands

The problem of high-resolution direction-of-arrival (DOA) estimation based on a limited amount of snapshots in automotive multiple-input multiple-output (MIMO) radar has been studied. The number of snapshots is restricted to minimize target spread/migration in range and/or Doppler domains. A computationally efficient approach for side-looking arrays is developed, which combines the generation of motion-enhanced snapshots and MIMO technology, thus exploiting the movement of the vehicle and the spatial diversity of the transmit and receive antennas. Due to motion, a larger virtual aperture is obtained and the angular resolution is boosted, achieving the separation of targets that the traditional MIMO approach cannot discriminate, as well as better results than with other single snapshot DOA estimation techniques. Algorithm performance has been studied in simulations, and possible limitations have been discussed. In addition, the method has been verified experimentally with pointlike and extended targets, and good agreement between simulations and experimental results has been observed.

Authors' addresses: Sen Yuan, Francesco Fioranelli, and Alexander G. Yarovoy are with the Microwave Sensing, Signals and Systems (MS3) Group, Delft University of Technology, Delft 2628 CD, The Netherlands, E-mail: (s.yuan-3@tudelft.nl; f.fioranelli@tudelft.nl; a.yarovoy@tudelft.nl). *(Corresponding author: Sen Yuan.)*

I. INTRODUCTION

Currently, a significant challenge in automotive is the development of advanced driver assistance systems (ADASs) for highly automated driving. These systems typically rely on sensors of different modalities: radars, cameras, and light detection and ranging (LiDARs) [1], as in general, no sensors can achieve comprehensive and accurate information on vehicle surroundings on their own. Radar technology has some unique advantages, namely the accurate and direct measurements of the range, relative velocity, and angle of multiple targets, and a long-range coverage of more than 200 m even in challenging weather or lighting conditions [2], [3]. Therefore, radar is typically one of the key technologies in current ADASs' tasks, such as adaptive cruise control (ACC) [4], forward collision avoidance [5], lane-change assistance [6], or evasion assistance [7] to name a few.

Autonomous driving requires high-resolution sensing capabilities, and thus, automotive radars must provide high-resolution information on the vehicle environment in the range-Doppler-azimuth-elevation domains. Because of their high degree of integration and low costs, radars operating in the 77-GHz band, known as mmWave frequencies, have become popular [8]. mmWave radar can offer a large operational bandwidth providing sufficient range resolution. Doppler resolution is a function of chirp duration and the number of chirps used for the estimation, so it is limited by the coherent observation time, with better velocity resolution achieved by operating at a higher frequency [9]. Angular resolution is contingent upon the antenna aperture and thus is determined by the number and placing of the transmit and receive antenna elements, limited by the radar cost and packaging size.

To obtain *high angular resolution*, large-aperture antenna arrays are created either via phased array [10], synthetic aperture radar (SAR) [11], or multiple-input-multiple-output (MIMO) array techniques [12]. Phased arrays typically use numerous half-wavelength spaced antennas to form a large aperture with a narrow beamwidth. However, they are not an economical option for civilian applications. SAR techniques form a large effective (i.e., virtual) aperture array by moving a small antenna or array that reduces the number of physical antennas required for imaging. This provides a cost-effective solution for high-resolution imaging applications but cannot be used efficiently in the forward direction. MIMO radar technology exploits the spatial diversity of transmit and receive antenna arrays and has received considerable attention in automotive. Due to its ability to achieve high angular resolution with a few antennas, MIMO has been exploited in current automotive radar for ADAS [13]. However, the practical implementation on vehicles constrains the radar size and limits the number of MIMO antennas.

In MIMO radar with a virtual uniform linear array (ULA), angle finding can be implemented via digital beamforming (DBF) [14] by performing computationally efficient fast Fourier transform (FFTs) on snapshots taken

across the array elements or using computationally intensive superresolution methods such as minimum variance distortionless response (MVDR) [15], and subspace-based methods, such as MUltiple SIgnal Classification (MUSIC) [16], [17] and estimation of signal parameters via rational invariance techniques [18]. All these methods require an input with a sufficient number of snapshots and assume a low mutual correlation of the sources and uncorrelated (white) noise [19], [20]. To obtain an accurate estimation of the array covariance matrix, spatial smoothing [16], [21] is applied to get enough virtual snapshots. Recent different approaches have also been reported, e.g., Guercan and Yarovoy [22] propose joint estimation using time-dependent steering vectors.

In this article, a novel approach to enhance the direction-of-arrival (DOA) estimation with the motion of the radar is proposed. Specifically, this article proposes a high angular resolution approach based on generating "motion-enhanced snapshots within a single frame," which is suitable for automotive side-looking or corner-placed radar. The velocity of the radar can be derived from the motion of the ego vehicle, which can be obtained with a global positioning system and different sensors. By combining the movement of the radar with the spatial diversity of the transmit/receive antennas, larger coherent virtual apertures can be formed and provide enhanced angular resolution. While some preliminary results are published in [23], in this article, the method is reformulated to work with a limited amount of snapshots and to deal with the cross-forward motion of the vehicle via a modified steering vector. Furthermore, the proposed method does not need any prior information on the characteristics of the environment or the targets in the scene, making it suitable for practical automotive applications.

Extending the array aperture with the movement of the radar has been researched in automotive applications. An approach forming a synthetic aperture for automotive MIMO radar has been explored in [24] and [25]. However, the methods in these studies can only enhance the resolution in their region of interest, i.e., the range of angles where targets have already been detected. Therefore, an additional processing step is needed to first detect the targets and estimate their related DOA values, which is then followed by the step of enhancing the angular resolution. The proposed method can directly image the targets in the radar field of view and use motion-enhanced snapshots (MSs) coherently to reduce the computational cost of the DOA estimation. Other studies propose to use the vehicle's trajectory to image the scenarios with the SAR approach. A two-radar approach is proposed in [26]. While one radar is used to determine the vehicle trajectory, another radar utilizes SAR on the known trajectory. This method uses back projection, which is an imaging algorithm with high computational load and less practical use while the proposed method uses a digital beam scan and compensates the extra vehicle movements with the modified steering vector. The work in [27] uses residual motion compensation to improve the SAR image quality for automotive but it should be noted that the aforementioned approaches still rely on snapshots across multiple frames.

Doppler beam sharpening methods are proposed for automotive radar in [28] and [29]. The velocity information was used for wideband DOA estimation with compensation of range migration and the presence of Doppler ambiguity [30] and for high angular resolution imaging [31]. Studies using neural networks have been proposed [32], [33], [34], [35] but despite their good results, the question of their generalization capabilities to unseen scenarios remains.

Other methods aim to perform *DOA estimation with a limited number of snapshots*, which is specifically attractive in automotive radar. Some snapshots may be distorted by interference and, thus, should not be used for DOA estimation while others may contain strong clutter and should also be avoided [36]. Furthermore, functionalities, such as ACC and emergency brake initiation require performing a very fast, online estimation of the relative distances, speeds, and DOA of targets. Hence, it is not uncommon in practice to use only a few usable snapshots for DOA estimation [13]. For example, the modified MUSIC in [37] uses the Hankel matrix to form the autocorrelation matrix for a single snapshot case. A 2-D convolutional neural network (CNN) has been proposed in [38] to achieve superresolution with a single snapshot but with results only verified in simulations. Sparse-sensing-based methods [39], [40] and IAA [41], [42], [43] are potentially applicable to a single snapshot or a limited number of snapshots but they both assume targets' sparsity and have high computational costs. Also, the Fourier interpolation methods proposed in [44] require the targets' sparsity to maintain acceptable performances. The reduced signal covariance matrix proposed in [19] operates on a limited amount of snapshots with unknown nonuniform noise but is affected by the rank deficiency problem and requires the prior number of targets. A purpose-designed array such as the massive ULAs in [45] focuses on improving DOA estimation with a few snapshots but is designed for communication applications rather than automotive. Sparse MIMO radar arrays as in [46] use genetic algorithms to interpolate the missing antennas in sparse arrays but this is computationally intensive. The aforementioned algorithms either need heavy computational load or a priori information, such as the number of targets in the scene, or do not take into account a variable time interval between the data acquisition periods. Alternatively, some ideas on how to create a large virtual aperture (i.e., the sum co-array and the array aperture extension) using sensor motion under very simplistic scenarios have been discussed in [47] and [48]. In this article, a novel formulation of the antenna array aperture extension due to platform motion is proposed. This includes a novel expression for the steering vectors to compensate for the error from the complex motion of the vehicle, a formulation with lower computational load via an approximation in the time tag, and a signal model accounting for the variable time interval for the data acquisition periods. To the best of our knowledge, this approach has allowed for the first-ever imaging of extended targets with a priori unknown number of scatterers by using the proposed aperture extension, target imaging with arbitrary movements of the radar

platform, and experimental demonstration with commercial radar with an arbitrary reset time between frames.

Summarizing, the main contributions of this article are as follows.

1) A high angular resolution DOA approach with low computational load is proposed by combining the vehicle's motion with automotive MIMO radar. The proposed method operates on a limited number of snapshots and includes the formulation of a modified steering vector to compensate for errors due to complex vehicle's motion and the approximation in the time tag.

2) The performance of the proposed method is analyzed in terms of its accuracy and probability of resolution and is shown to outperform alternative approaches from the literature. For the first time in the literature, a detailed analysis of the impact of forward and cross-forward velocity estimation errors on the performance of the DOA method has been performed. Both simulated data from pointlike and complex extended targets, as well as on experimental data, have been used in the method performance analysis.

The rest of this article is organized as follows. In Section II, the signal model for DOA estimation based on moving FMCW MIMO radar is provided. The problem formulation and the proposed method, as well as the modified steering vector for the proposed method, are demonstrated in Section III. Simulation results for ideal point targets and complex extended targets, as well as the experimental tests, are provided in Section IV. Finally, Section V concludes this article.

II. SIGNAL MODEL FOR DOA ESTIMATION BASED ON MOVING FMCW MIMO RADAR

A. Signal Model

Frequency-modulated continuous wave (FMCW) MIMO radar is assumed with $M_{\mathbf{t}}$ transmit and $M_{\mathbf{r}}$ receive antennas, equivalent to a radar with virtual uniformly distributed linear array (ULA) of $M_{\mathbf{t}}M_{\mathbf{r}}$ elements. The index of the transmit antenna elements is denoted by $q \in [0, M_{\mathbf{t}}]$, and the index of the receive antenna elements is denoted by $p \in [0, M_{\mathbf{r}}]$. Subsequently, the index of the resulting virtual ULA is dependent on the MIMO geometry and denoted by $a \in [0, M_{\mathbf{t}}M_{\mathbf{r}} - 1]$.

The FMCW chirp is transmitted with duration T_c, bandwidth B, and pulse repetition interval (PRI) T and has the form

$$s_0(t) = \begin{cases} e^{j2\pi\left(f_0 t + 0.5\mu t^2\right)}, & t \in [0, T_c] \\ s_{\text{settle}}(t), & t \in [T_c, T] \end{cases} \quad (1)$$

where f_0 denotes the starting frequency, $\mu = B/T_c$ denotes the frequency modulation rate, and $s_{\text{settle}}(t)$ indicates the signal during the settling time of the radar.

The periodic transmitted signal is decomposed into fast-time domain t' and chirp number domain $l = \lfloor \frac{t}{T} \rfloor$ with $t' = t - lT$, $t' \in [0, T_c]$. The notation $\lfloor \rfloor$ indicates the rounding

operation to integer; hence, $l = 0, 1, 2, \ldots, L_d - 1$, where L_d is the total number of the chirps in one frame. Thus, the periodic sequence of chirps can be expressed as

$$s(t) = s\left(t' + lT\right) = s\left(l, t'\right) = s_0\left(t'\right). \quad (2)$$

The multitarget signal will be the summation of the single-point target's signals. To illustrate the signal model, the radar signal is derived first based on the single-point target's signal and extended to a multitarget at the end. The round trip delay of the reflected signal for the $\mathbf{o}$ target and the ath antenna element in the MIMO ULA is

$$\begin{aligned} \tau_{\mathbf{o}}\left(l, t'\right) &= \frac{2\left(D_{\mathbf{o},a}(t' + lT) + v_r\left(t' + lT\right)\right)}{c} \\ &\approx \gamma_{\mathbf{o}} + \frac{2v(t' + lT)}{c} \end{aligned} \quad (3)$$

where c is the speed of light, $D_{\mathbf{o},a}(t)$ is the range between $\mathbf{o}$-target and the ath antenna at time t, v_r is the radial velocity between the radar and the target, and $\gamma_{\mathbf{o}} = \frac{2D_{\mathbf{o},a}(t' + lT)}{c} \ll T_c$. The corresponding received signal can be written as

$$\begin{aligned} r_{(\mathbf{o},a)}(l, t') &= \alpha_{\mathbf{o}} e^{j\phi_{\mathbf{o},a}} s\left(t' + lT - \tau_{\mathbf{o}}(l, t')\right) \\ &\quad \text{with } t' \in [\gamma_{\mathbf{o}}, T_c] \end{aligned} \quad (4)$$

where $\alpha_{\mathbf{o}}$ is the constant complex amplitude related to the characteristics of the target $\mathbf{o}$, and $e^{j\phi_{\mathbf{o},a}}$ denotes the phase delay of the ath antenna.

A property of the virtual ULA is that the range difference between target and different receive antenna pairs will be approximately equal to a constant with respect to the DOA

$$D_{\mathbf{o},a}(t) - D_{\mathbf{o},a+1}(t) \approx d \sin \theta_{\mathbf{o}} \quad (5)$$

where $d = \lambda/2$ is the distance between different receive antennas, λ is the wavelength, and $\theta_{\mathbf{o}}$ is the azimuth angle of the target $\mathbf{o}$ counted from the virtual array broadside direction.

Then, the phase delay of the ath antenna relative to the 0th element in the ULA for the target $\mathbf{o}$ is obtained by

$$\phi(\mathbf{o}, a) = 2\pi f_{\mathbf{0}} \frac{ad}{c} \sin \theta_{\mathbf{o}}. \quad (6)$$

The received signal is then correlated with the conjugate copy of the transmitted signal $s^*(l, t')$ to obtain the dechirped signal $z_{\mathbf{o}}$ as

$$z_{\mathbf{o}}\left(a, l, t'\right) = r_{(\mathbf{o},a)}\left(l, t'\right) \times s^*\left(l, t'\right). \quad (7)$$

This signal will be sampled with respect to fast-time with frequency f_s and the discretized signal $\hat{z}_{\mathbf{o}}$ in the time domain is obtained as

$$\begin{aligned} \hat{z}_{\mathbf{o}}(a, l, k) &\approx \alpha_{\mathbf{o}} \exp\Big[j\phi\left(\mathbf{o}, a\right) \\ &\quad - j2\pi\left(f_{d,\mathbf{o}}Tl + \mu \frac{D_{\mathbf{o},a}(l)}{c}\frac{k}{f_s}\right)\Big] \end{aligned} \quad (8)$$

$k = 0, 1, 2, \ldots, K_d - 1$ where $K_d = T_c f_s$ is the maximum number of samples within one chirp, $f_{d,\mathbf{o}} = \frac{2v_{r\mathbf{o}}f_0}{c}$ is the Doppler frequency of the target $\mathbf{o}$, and $v_{r\mathbf{o}}$ is the radial velocity of the target $\mathbf{o}$. When the number of the scatter
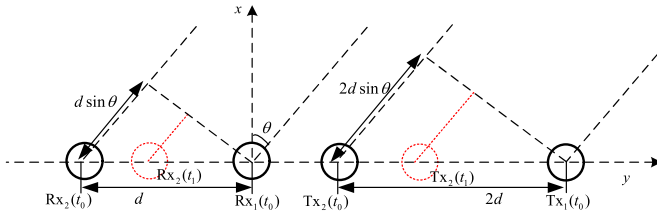
Fig. 1.   Geometrical configuration of the MIMO approach, where the solid black line shows the MIMO antennas at time t_0, and the red dotted line shows the antennas at time t_1 after the movement of the vehicle.

TABLE I
Range Relationship of Different 2×2 MIMO
Antenna Pairs

Range	0	$d \sin \theta_{\mathbf{o}}$
Tx–Rx pairs	$D_{\mathbf{o},0}(t_0)$	$D_{\mathbf{o},1}(t_0)$
Range	$2d \sin \theta_{\mathbf{o}}$	$3d \sin \theta_{\mathbf{o}}$
Tx–Rx pairs	$D_{\mathbf{o},2}(t_0)$	$D_{\mathbf{o},3}(t_0)$

points in the field of view is equal to k_s, the total signal is constructed by superposition

$$\hat{z}(a, l, k) = \sum_{\mathbf{o}=1}^{k_s} \hat{z}_{\mathbf{o}}(a, l, k). \tag{9}$$

B.   Geometry Model for the Radar Movement

A generic 1-D MIMO array placed in the y-direction is considered, with the x-axis pointing toward the illuminated scene and assuming no movement in the z-axis, as shown in Fig. 1. The platform where the radar is installed is moving along the y-axis at speed $v(t) = [0, v_y(t), 0]$, with static objects located in the far-field of the MIMO array. Using a two-transmit and two-receive antenna MIMO array as an example, as shown in Fig. 1 with a solid line, the virtual aperture array can be formed with four antennas with range relationships as shown in Table I. Here, $\mathbf{o}$ refers to a target and $\theta_{\mathbf{o}}$ is its azimuth angle.

Inspired by SAR approaches, finer angular resolution can be obtained by exploiting the movement of the vehicle to expand the MIMO virtual aperture. For example, in Fig. 1, after moving in a short time from t_0 to t_1, the target will remain in the same position while the transmit and receive antenna in a black solid line marked with $\mathbf{R}x_2$ and $\mathbf{T}x_2$ will arrive at the positions marked with the red dotted lines. When the vehicle is moving with velocity v_y, each antenna will move by a range equal to $v_y|t_1 - t_0|$ along the antenna direction-y. Because of the two-way propagation, the difference in range between the target $\mathbf{o}$ and the ath antenna moving position from time t_0 to t_1 will be calculated as in (10). Essentially, this equation is similar to (5) but with the difference in range to the target calculated between the same antenna a moving with the vehicle's velocity at two time steps, rather than between two separate antennas at the same time step

$$D_{\mathbf{o},a}(t_0) - D_{\mathbf{o},a}(t_1) = v_y \frac{|t_1 - t_0|}{2} \sin \theta_{\mathbf{o}}. \tag{10}$$
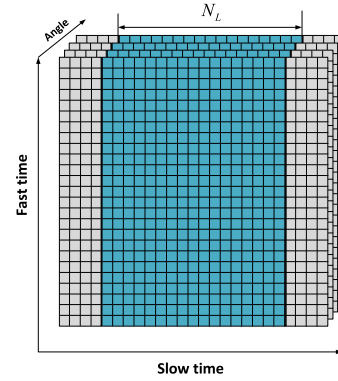

Fig. 2.   Sketch of the "*limited amount of snapshots*," with the 3-D tensor with slow time, fast time, and angle axes. The whole tensor depicts one frame, where the blue region includes the snapshots used for DOA estimation.

III.   PROPOSED DOA ESTIMATION BASED ON A LIMITED AMOUNT OF SNAPSHOTS

A.   Fundamentals of the Proposed Approach

The array response at a specific time instance with data obtained at all the virtual receivers and corresponding to the same range-Doppler bin is defined as the *array snapshot* [13].

For side-looking radar on a vehicle, the target Doppler velocity is mainly related to the vehicle's movement; hence, the target Doppler cell will remain the same within one frame. However, to maintain the DOA coherency, i.e., ensuring that targets remain in their range bins during processing, only a limited number of snapshots N_L can be used for DOA estimation. This number is determined by the relative speed and the range resolution as

$$N_L = \frac{\frac{c}{2B}}{T \, |v_r|} \tag{11}$$

where v_r is the radial target velocity caused by the vehicle's speed. It should be noted that for MIMO automotive radar working with time division multiple access mode, the PRI T in (11) will be multiplied by the number of transmitters, making N_L smaller. For this limited amount of snapshots N_L, the 3-D data tensor (shown in Fig. 2) can be expressed as in (9). The first dimension is related to the angle estimation, the second to the velocity estimation, and the third to the range estimation.

As well known, only a coherent virtual aperture can improve angular resolution. This means that extra virtual antennas generated from the vehicle's movement are only usable for DOA estimation when the phase differences caused by such movement are the same as the phase difference between adjacent MIMO virtual ULA elements.

Here, for simplicity, we use the 2×2 MIMO in Fig. 1 for demonstration. This means that t_1 and t_0 must satisfy the following equation to make the formed aperture coherent:

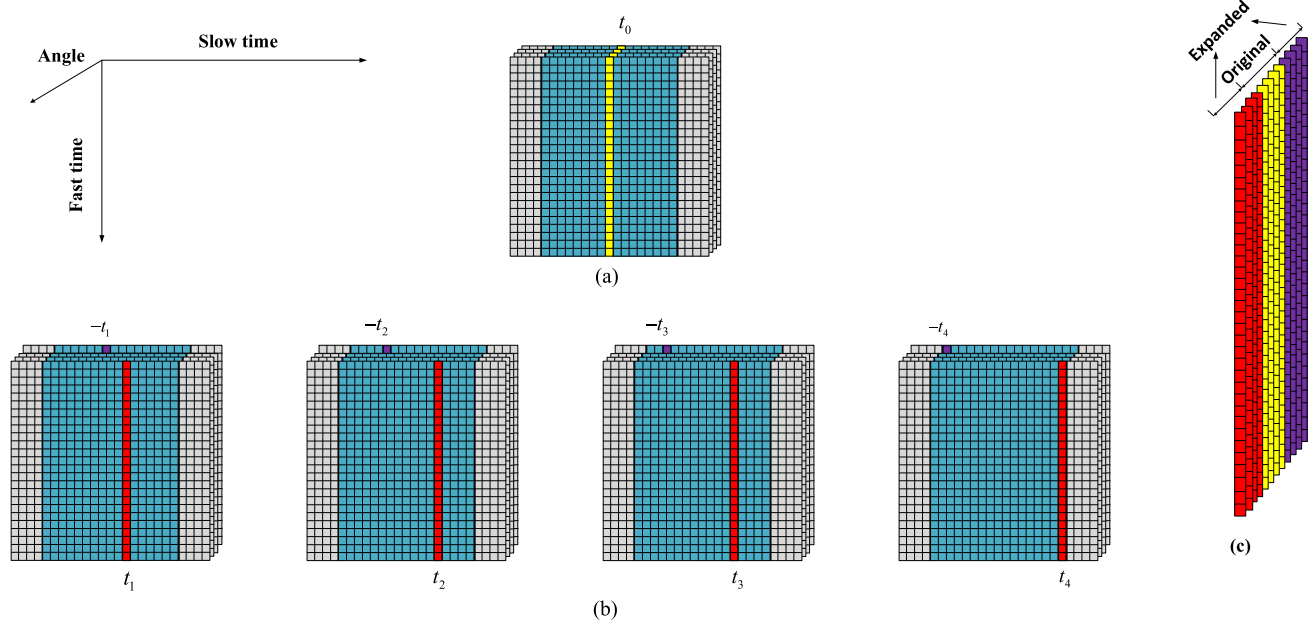$$2v_r(t_1 - t_0) = d \sin \theta_{\mathbf{o}}. \tag{12}$$

Fig. 3. Principle of the proposed method. (a) OS (in yellow color) taken from the middle of the group of snapshots usable for DOA also shown in Fig. 2. (b) MSs (in red and purple colors) derived from the same group of snapshots in a frame. (c) New "DOA snapshot" formed by combining OS and different MSs according to the proposed method.

It appears from this equation that the coherency relation depends on the position of the target $\mathbf{o}$, i.e., on $\theta_{\mathbf{o}}$. However, considering only the Y component of the velocity assuming that the effect of the other components is compensated (as described in the next section), then $v_r = v_y \sin \theta_{\mathbf{o}}$. This removes the dependence on θ from (12). Also, when the aperture is extended with the proposed method, then (12) becomes

$$t_i = t_0 + iT_{\text{ind}}, i \in \mathbb{Z} \quad (13)$$

where $T_{\text{ind}} = \lfloor \frac{d}{2v_y T} \rfloor T$ is the approximate time tag interval for a coherent aperture extension. To satisfy the constraint of an integer slow time index, the $\lfloor \rfloor$ rounding operation is implemented here, thus introducing an approximation error.

If the time step satisfies (13), (10) for the 2×2 MIMO taken as an example will become

$$D_{\mathbf{o},a}(t_0) - D_{\mathbf{o},a}(t_1) = d \sin \theta_{\mathbf{o}}. \quad (14)$$

This relation linking the range difference between the same antenna position moving from time t_0 to t_1 and DOA angle $\theta_{\mathbf{o}}$ is the same as the range difference between adjacent Tx–Rx pairs, as shown in (5). Essentially, by calculating a suitable time tag as in (13), the movement of the vehicle can be exploited to coherently extend the original MIMO virtual array.

A graphical representation of the proposed approach is shown in Fig. 3. One snapshot (marked by the yellow color) is chosen in the middle of the N_L received snapshots usable for DOA estimation. This initial snapshot $\hat{S}(t_0)$ is named "original snapshot (OS)" and is defined starting from (9) as

$$\hat{S}(t_0) = \hat{z}(:, t_0, :). \quad (15)$$

As shown in Fig. 3(a), this choice provides the largest space for generating "motion-enhanced snapshots (MS)" to coherently expand the OS $\hat{S}(t_0)$. Essentially, as shown in Fig. 3(b), the MS in red color $\hat{S}(t_i)$ is generated from the first transmitter and receiver with a positive time tag. In contrast, the MS in purple color $\hat{S}(t_{-i})$ is generated from the last transmitter and receiver with a negative time tag. These MSs are expressed as

$$\hat{S}(t_i) = \hat{z}(1, t_i, :)$$
$$\hat{S}(t_{-i}) = \hat{z}(M_t M_r, t_{-i}, :). \quad (16)$$

After generating multiple MSs, a new range-angle matrix $\mathbf{S}(t)$ can be formed as shown in Fig. 3(c). The OS is located in the middle of the matrix with a length of $M_{\mathbf{t}}M_{\mathbf{r}}$ in the dimension associated with the angle/DOA while the MS is located to the left and right part with a total length of N_{ex}. Therefore, the new, extended range-angle matrix will have a length of $M_{\mathbf{t}}M_{\mathbf{r}} + N_{\text{ex}}$ in the dimension associated with the angle/DOA, which is essentially equivalent to having additional, multiple channels for DOA estimation. The matrix $\mathbf{S}(t)$ can be written as in (17), with its rows corresponding to angle vectors over which DOA estimation can be performed

$$\mathbf{S}(t) = \underbrace{[\hat{S}(t_{-\frac{N_{\text{ex}}}{2}}), \ldots \hat{S}(t_{-i}), \ldots, \hat{S}(t_0), \ldots, \hat{S}(t_i), \ldots, \hat{S}(t_{\frac{N_{\text{ex}}}{2}})]}_{M_{\mathbf{t}}M_{\mathbf{r}}+N_{\text{ex}}}$$

$$(17)$$

where N_{ex} is the number of additional channels in the aperture formed with the proposed method. This larger aperture improves the resulting angular resolution.

B. Modified Steering Vector

After range FFT, the rows of the matrix $\mathbf{S}(t)$ can be considered as angle vectors for DOA estimation. For a given range bin, i.e., a given row, the contributions from targets located at the corresponding range will be superimposed. This can be modeled as a linear combination of incident signals from each target and zero mean Gaussian noise, where the incident signals are assumed to be in a direct line of sight and uncorrelated with the noise. Hence, the angle column vector $\mathbf{X}$ for a given range bin can be expressed as

$$\mathbf{X} = \sum_{m=1}^{M} a(\theta_m) s_m(t) + n(t) = \mathbf{A}\mathbf{S}_t + \mathbf{N} \in \mathbb{C}^{(M_t M_r + N_{\text{ex}}) \times 1} \tag{18}$$

where M indicates the number of incident signals on the array, $s_m(t)$ is an $M \times 1$ vector of a source waveform for the mth source at the direction θ_m from the array boresight and can be written with matrix multiplication with $\mathbf{S}_t$. $a(\theta_m)$ is the $(M_t M_r + N_{\text{ex}}) \times 1$ steering vector or response vector of the array for the angular direction θ_m. $\mathbf{A}$ is a $(M_t M_r + N_{\text{ex}}) \times M$ matrix of steering vectors

$$\mathbf{A} = [\mathbf{a}(\theta_1), \quad \mathbf{a}(\theta_2), \quad \mathbf{a}(\theta_3), \quad \ldots \quad , \mathbf{a}(\theta_M)] \tag{19}$$

$$\mathbf{a}(\theta_{\mathbf{m}}) = \left[1, e^{-j2\pi d \sin \theta_m / \lambda}, \ldots, e^{-j2\pi (M_t M_r + N_{\text{ex}} - 1) d \sin \theta_m / \lambda}\right]^T \tag{20}$$

where $[\bullet]^T$ denotes the operation of matrix transpose. With the proposed method, for our generated array with motion enhancement, the steering vector is given by

$$\mathbf{w}(\theta) = \left[1, e^{-j2\pi d \sin \theta / \lambda}, \ldots, e^{-j2\pi (M_t M_r + N_{\text{ex}} - 1) d \sin \theta / \lambda}\right]^T. \tag{21}$$

However, in our proposed method, in order to obtain an integer slow time tag, the rounding operation is implemented in (13), thus introducing an extra time delay as

$$t_e(i) = \frac{d}{2v_y} - (t_i - t_0). \tag{22}$$

This time delay will cause an error equivalent to an extra movement in the forward direction, thus leading to a phase error. For each MS formed with the proposed method, the resulting phase error can be written as

$$w_{ea}(\theta, i) = e^{-j2\pi 2 v_y \times t_e(i) \sin \theta / \lambda} \tag{23}$$

where i is the index in the calculation of the time tag defined in (13).

Furthermore, the motion of the vehicle will be more complex than linear motion in one direction, i.e., there can be cross-forward movements during driving. This extra velocity component v_x will introduce an additional phase shift as

$$w_{ev}(\theta, i) = e^{-j2\pi v_x \times (t_i - t_0) \cos \theta / \lambda}. \tag{24}$$

Combining the two aforementioned sources of error, a compensation factor for the original steering vector in (21) can be written as

$$w_e(\theta, i) = w_{ea}(\theta, i) w_{ev}(\theta, i). \tag{25}$$

It should be noted that this compensation is only needed for the additional MSs generated by the movement of the vehicle but not for the OS.

Finally, the modified new steering vector will be expressed as

$$\mathbf{w}_w(\theta) = \mathbf{w}(\theta) \odot \left[w_e\left(\theta, -\frac{N_{\text{ex}}}{2}\right), \ldots, w_e(\theta, -i), \ldots, \right.$$
$$\left. \mathbf{w}_e(\theta, 0), \ldots, w_e(\theta, i), \ldots, w_e\left(\theta, \frac{N_{\text{ex}}}{2}\right)\right]^T \tag{26}$$

where $\odot$ is the Hadamard product. $\mathbf{w}_e(\theta, 0)$ is the unit vector with length $M_t M_r$, recalling that the OS does not need any compensation. After concatenating the vector with the other scalars derived from (25), the total length would be $M_t M_r + N_{\text{ex}}$, the same as the range-angle matrix in (17).

C. Summary of the Proposed Algorithm

Step 1: Expand the amount of snapshots for DOA estimation based on the movement of the vehicle.

As discussed in Section III-A, those snapshots (MSs) coherent with respect to the original MIMO virtual ULA are selected as in (13). Then the new group of snapshots for DOA estimation $\mathbf{S}$ can be obtained by concatenating OS and MSs in a range-angle matrix, as in (17).

Step 2: Compensate the phase error in the steering vector.

As discussed in Section III-B, the approximation error in the calculation of an integer time tag and the error due to the presence of additional cross-range velocity components need compensation. Those errors will translate to the phase domain, and the compensation is performed by the term (25). Hence, the final modified steering vector $\mathbf{w}_w(\theta)$ is formed as in (26).

Step 3: DOA estimation based on the new formed range-angle matrix $\mathbf{S}$ and modified steering vector $\mathbf{w}_w(\theta)$.

$\mathbf{S} \in \mathbb{C}^{K_d \times (M_t M_r + N_{\text{ex}})}$ defined in (17) is a range-angle matrix with K_d rows corresponding to fast time samples and $M_t M_r + N_{\text{ex}}$ columns corresponding to the equivalent number of channels to perform DOA estimation. After performing FFT along the fast-time for range estimation, each row of the matrix containing detected targets can be considered as an angle column vector to perform DOA estimation as in (18). For a given range index with detected targets, the DBF algorithm can perform the DOA estimation on the corresponding angle column vector $\mathbf{X}$ defined in (18). The received power $P_{\text{DBF}}(\theta)$ at each angle can be expressed as [49]

$$P_{\text{DBF}}(\theta) = \frac{\mathbf{w}_w^H(\theta) R_{\mathbf{XX}} \mathbf{w}_w(\theta)}{\mathbf{w}_w^H(\theta) \mathbf{w}_w(\theta)} \tag{27}$$

where $R_{\mathbf{XX}} = E[\mathbf{X}\mathbf{X}^H]$ is the autocorrelation matrix of $\mathbf{X}$, and the notation $[\bullet]^H$ denotes the operation of conjugate transpose.

The algorithm is summarized in "Algorithm 1."

Algorithm 1: Proposed DOA Estimation Algorithm.

Calculate the time tag t_i as in (13).

Expand the amount of snapshots for DOA estimation, generating the range-angle matrix **S** as shown in (17).

Compute the modified steering vector $\mathbf{a_w}(\theta)$ as in (26).

Compute the angle column vector **X** for the range of a detected target.

for θ in $[-90°, 90°]$ **do**

$\quad R_{\mathbf{XX}} = E[\mathbf{XX}^H]$

$\quad P_{DBF}(\theta) = \frac{\mathbf{w}_w^H(\theta)R_{\mathbf{XX}}\mathbf{w}_w(\theta)}{\mathbf{w}_w^H(\theta)\mathbf{w}_w(\theta)}$

endfor

Fig. 4.   MSE and CRLB for the DOA estimation of different algorithms in different SNR conditions.

D.   Possible Limitations

Possible limitations can come from the memory size of the radar, its transmission rate, or the snapshot number in (11). They will influence the snapshot size in the Doppler dimension, which limits the maximum number of MS N_m, we can form

$$N_m = \left\lfloor \frac{\min(L_d, N_L)}{\left\lfloor \frac{d}{2v_yT} \right\rfloor} \right\rfloor \tag{28}$$

where L_d is the total number of chirps in one snapshot, d is the distance between different receivers, T is the chirp duration.

The proposed method also requires enough movement to expand the aperture during the snapshots' period. This is highly related to the vehicle speed and the radar chirp duration in (13). The requirement for the vehicle speed is

$$V_v \in \left[\frac{d}{4\min(L_d, N_L)T_c}, \frac{d}{2T_c} \right]. \tag{29}$$

Typical values of the speed for vehicles are in the range of approximately $[0.1, 117]$km/h. According to the 77 GHz automotive radar parameters in [50] and [51], for a normal speed in urban areas of 40 km/h; for example, the maximum amount of MS will be 40. To obtain a useful aperture size, the cross-range speed should satisfy $v_x \ll v_y\tan(\theta)$, where θ is the target azimuth angle. The acceleration of cars is not expected to have a large impact as the duration of the frame is relatively small. According to the work in [52], the maximum acceleration of cars is 2.87 m/s^2, which will lead to 0.01 m/s in velocity difference within a snapshot.

IV.   RESULTS AND DISCUSSION

To show the effectiveness of the proposed method, results based on simulated ideal point targets, simulated complex extended targets, and experimental data are presented in this section. It is shown that targets overlapped together in an angular domain are separated successfully by our method based on a limited amount of snapshots.
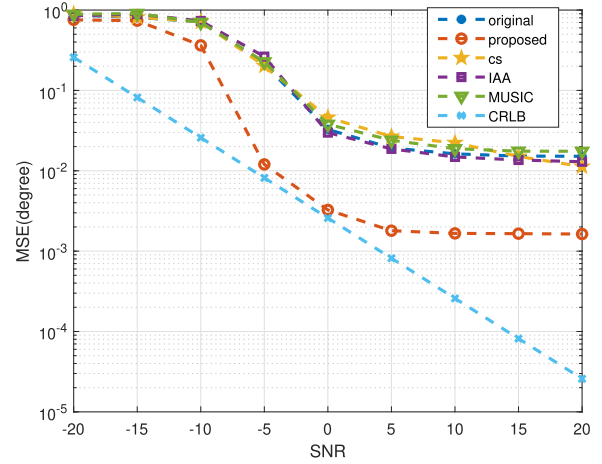
A.   Ideal Point Targets

We used a simulated 2×4 MIMO radar for azimuth DOA estimation, comparable to commercial mmWave modules operating at 77 GHz. The specifications of the radar parameters are listed as follows: the starting frequency of the FMCW chirp f_0 is 77 GHz, the chirp bandwidth B is 1 GHz, the chirp duration T_c is 30 μs, the sampling rate f_s is 34 Ms/s, and $L = 256$ chirps are processed in each frame. The MIMO antenna on the side-looking radar was located at the coordinate center.

The Cramér–Rao lower bound (CRLB) on the accuracy of the DOA estimation in white noise has already been derived in the literature [53] as

$$\text{CRLB}(\theta) = \frac{\sigma}{2}\{Re[\mathbf{X}^H(\theta)\mathbf{D}^H(\theta)$$
$$\left[\mathbf{I} - \mathbf{a}(\theta)(\mathbf{a}^H(\theta)\mathbf{a}(\theta))^{-1}\mathbf{a}^H(\theta)\right]\mathbf{D}(\theta)\mathbf{X}(\theta)]\}^{-1} \tag{30}$$

where σ is the noise power obtained from a given SNR, $\mathbf{a}(\theta)$ is the steering vector, $\mathbf{D}(\theta) = d\mathbf{a}(\theta)/d\theta$, and $\mathbf{X}(\theta)$ is a diagonal matrix whose diagonal elements describe the ground truth of the simulated targets.

A comparison between the MSEs of the five considered beamformers, namely original beamscan, proposed method, IAA-APES [42], single-snapshot MUSIC [37], and compressed sensing [39] using CVX tools [54] for a limited amount of snapshots (i.e., 128 snapshots) is shown in Fig. 4 with the CRLB. Here, only one target is considered at a random position, and the number of independent Monte Carlo trials to generate this figure was 10^3. The MSE figure clearly demonstrates the different beamformers' DOA performance in terms of their accuracy. As expected the performance of all beamformers drops with increasing SNR but the proposed method outperforms the other approaches from the literature. Furthermore, a comparison between the CRLB and the proposed DOA method at SNR equal to 6 dB with different values of the expand number N_{ex} is shown in Fig. 5, as well as the CRLB of the original array. The CRLB corresponds to the ULA with a size equal to the virtual
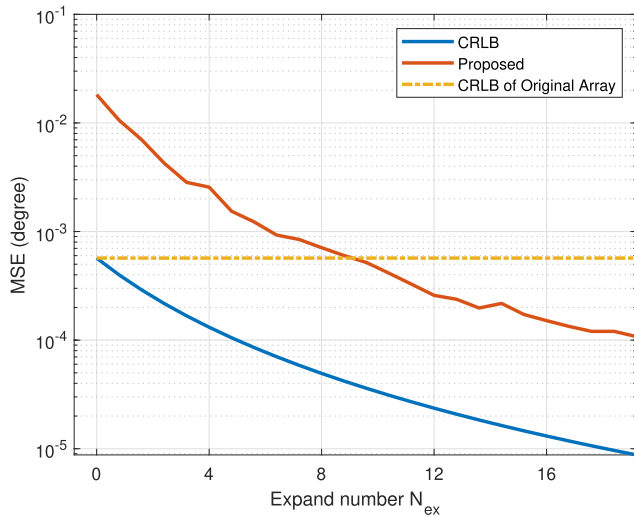
Fig. 5. CRLB and MSE of the DOA estimation with the proposed method with a different limited amount of snapshots for different aperture sizes.

Fig. 7. Simulated performance comparison of different methods for two targets scenario when two point targets are located at $10°$ and $16°$.
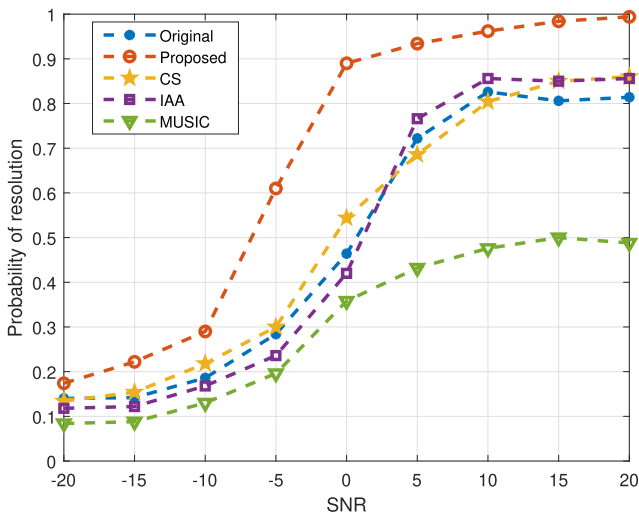

Fig. 6. Probability of resolution of different algorithms under different SNR conditions.

aperture formed by exploiting the movement of the vehicle with the proposed method. One can observe that with N_{ex} equal to 9, the proposed method reaches the CRLB level of the original array. The MSs formed by the proposed method give the ability to approach and even break the CRLB for the current number of antennas.

Additionally, the probability of resolution for the different DOA algorithms at different SNR values is shown in Fig. 6. The simulations are performed following this procedure: Two targets are placed randomly in the range $[-40°, 40°]$; the number of independent Monte Carlo trials is 500; only those simulations that can separate two targets successfully will be added to the probabilities' numerator. The figure shows that the proposed method achieves the best resolution ability in different SNR conditions while the single snapshot MUSIC is the worst. It should be noted that DOA estimation algorithms are, in general, applied in
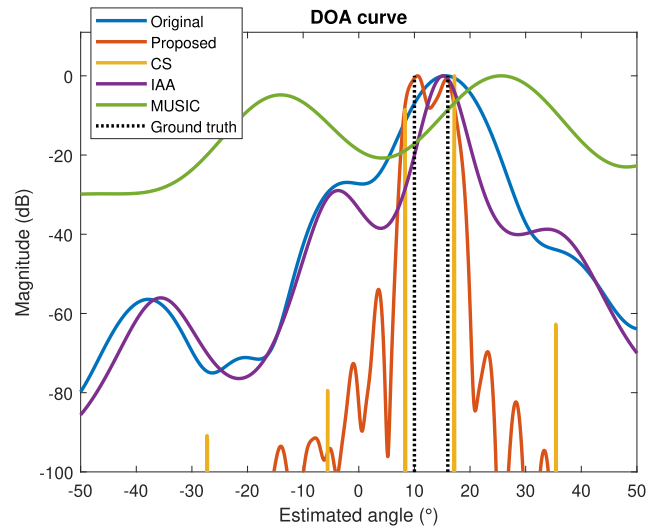
relatively high SNR conditions [24]; for example, commercial radar units such as those by Bosch or Conti are both evaluated on SNR = 20 dB. This is reasonable for automotive radar scenarios because it is more important to separate in angle closer targets (hence with higher SNR values) than targets further away (hence detected at lower SNR). So under high SNR, the probability of resolution almost reaches the value of 90% with the proposed method.

To provide a further comparison of the performances of different methods, a case where two targets are located at $10°$ and $16°$ is shown in Fig. 7. The MIMO array on the side-looking radar is located at the coordinate center, with targets placed at the same range bin of 10 m to meet the Fraunhofer distance requirement [55] and ensure that they are in the far-field of the array. The radar moves with velocity $v_y = 10$ m/s, and the SNR is set to 20 dB. From Fig. 7, one can observe that in this specific case, the proposed method and the CS-based method separate both targets successfully while other methods fail to do so. Also, the proposed method provides DOA estimations equal to $10.6°$ and $15.8°$ while the CS-based method estimates the target DOA less accurately: $8.3°$ and $17.2°$.

The above results demonstrate that the proposed algorithm provides the best estimate of the targets' angles with a limited amount of snapshots, both in terms of accuracy and resolution capability. It is important to mention that no prior information about the targets is needed for the proposed method compared to compressed-sensing-based methods.

In terms of *computational complexity*, a Monte Carlo test as well as a theoretical analysis has been reported here. The expressions of the computational complexity for the proposed method are $O((m^2 + 2m)N)$, for the MUSIC method is $O(m^3 + (2mn + m)N + m(log_2 m))$, and for the CS method based on CVX is $O(m^{3.5} ln(\epsilon))$, where m is the number of snapshots used, N is the number of the antennas, n is the number of targets which is required for MUSIC, ϵ is the duality gap defined in the primal–dual interior-point
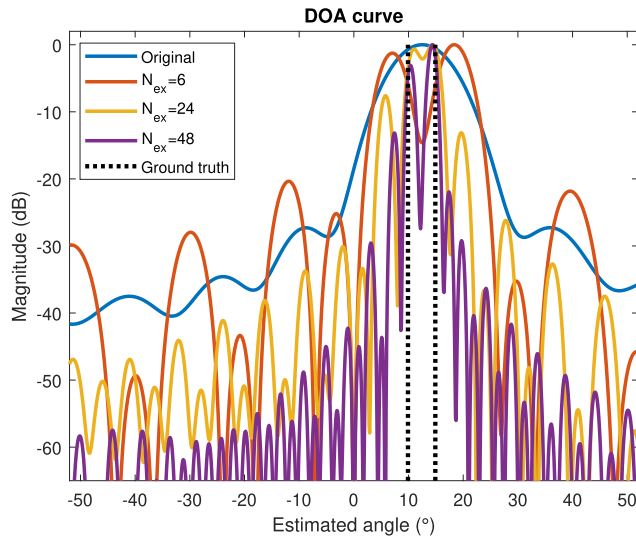
Fig. 8. Simulated performance comparison of the proposed limited amount of snapshots' method versus the original beamscan method, with different aperture sizes. The two-point targets are located at 10° and 15°.

Fig. 9. Box-plot for DOA estimation error from a 500-repetitions Monte Carlo test with different aperture sizes (parameter N_{ex} described in Section III). The central mark in the blue box indicates the median, and the bottom and top edges of the box indicate the 25th and 75th percentiles, respectively. The whiskers extend to the most extreme data points considered as outliers, and the outliers are plotted individually using the "+" marker symbol.

algorithm of the CVX formulation [56]. Thus, the computationally complexity of the method proposed grows much slower with the number of snapshots than for the reference methods and—in contrary to MUSIC—the computational complexity is independent of the number of targets. Also, Monte Carlo tests were performed with random positions of two targets located in the same range bin for each test to estimate the average time taken to compute one 1D DOA for each algorithm. Specifically, 500 repetitions are considered for implementation in MATLAB on a standard desktop computer, common to all the considered algorithms. In terms of computation time, the original MIMO beamscan takes 10 ms, the compressed sensing-based algorithm takes 1014 ms, the single-snapshot MUSIC takes 323 ms and the IAA-based takes 2072 ms, whereas the proposed method with $N_{ex} = 48$ only needs 56 ms to generate the DOA results. Compared with other algorithms in the literature, the proposed approach is the fastest to achieve the DOA estimation. The computational time increases if an increasing number of snapshots is used but with very good performances. For example, while using the proposed method with $N_{ex} = 48$ increased the computational time, this is only about five times larger than the original MIMO beamscan (56 ms versus 10 ms); however, the performance in terms of both resolution and accuracy is significantly improved, as shown in Figs. 4 and 6.

To test the impact of the parameter N_{ex}, the same scenario where the two targets are located at 10° and 15° is analyzed. When the radar moves with velocity $v_y = 5$ m/s, the results of the proposed approach with $N_{ex} = 6, N_{ex} = 24,$ and $N_{ex} = 48$ are compared with the original beamscan method. From Fig. 8, we can see that the proposed approach starts separating the two targets, and when increasing the aperture with a higher expand number, the beam becomes narrower and the DOA estimation is more accurate. In contrast, the original beamscan method cannot separate the
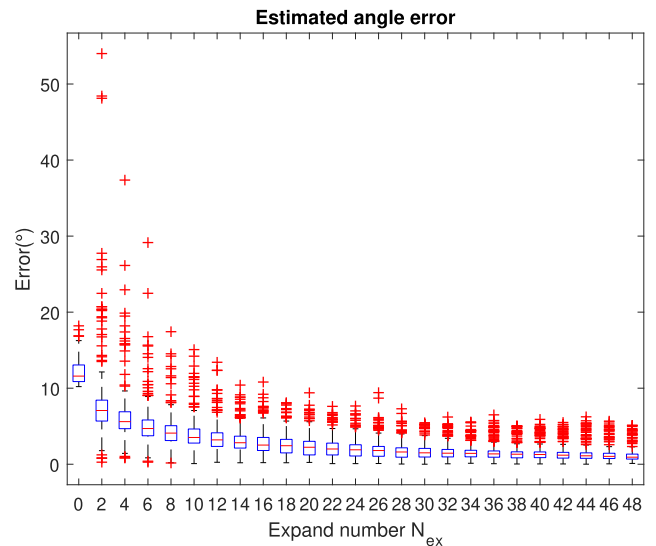
targets and only estimates one single target approximately in the middle of the ground truth locations. In order to test the resolution ability more comprehensively, a Monte Carlo simulation for two close targets located at random positions is performed, and the data are processed for different expand number N_{ex} with results shown in Fig. 9. There is more error spread and outliers with smaller values of N_{ex}. As larger apertures are generated with higher N_{ex}, the mean value of the error for the DOA estimation of the two targets decreases.

As discussed in the preliminary results in [23], the performance of the proposed method will yield a better estimation with lower speed and shorter chirp duration but is more sensitive to the speed fluctuation or chirp duration uncertainty. For the simulated setting in this article (the nominal vehicle velocity is equal to 5 m/s), the analysis in (31) shows that if the actual velocity is within this interval, $v_y \in [4.69, 5.73]$m/s; then, the time index in (13) will be the same, providing the correct DOA estimation. Similarly, if the nominal radar speed becomes 9 m/s, then the tolerance interval to maintain reliable DOA estimation will become $v_y \in [7.4, 10.3]$ m/s

$$v_{min} = \left\lfloor \frac{d}{2(T_{ind} + 0.5)T} \right\rfloor T$$

$$v_{max} = \left\lfloor \frac{d}{2(T_{ind} - 0.5)T} \right\rfloor T. \qquad (31)$$

The platform motion in automotive is usually more complicated than a simple one-dimensional translational movement. The error due to this complex motion can be further compensated in the steering vector for our proposed method, as discussed in Section III-B. As an example, the
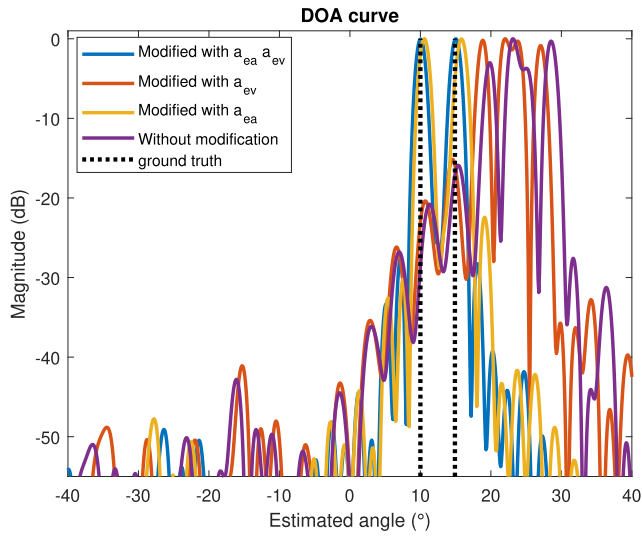
Fig. 10. Influence of the modified steering vectors for error compensation on the DOA estimation. Ground-truth target positions are indicated by the black lines.
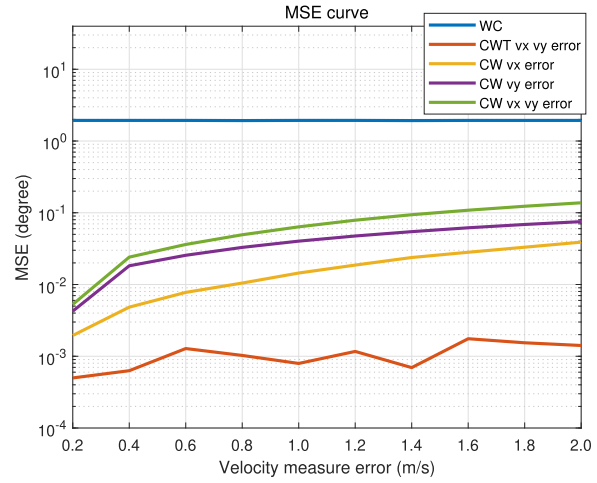

Fig. 11. MSE for the DOA estimation with or without compensation based on the modified steering vector with respect to different velocity measure errors. WC refers to the estimation without any compensation based on the modified steering vector; CWT refers to the estimation with compensation based on the modified steering vector but without velocity measure errors; CW refers to the estimation with compensation based on the modified steering vector in the presence of velocity measure errors.
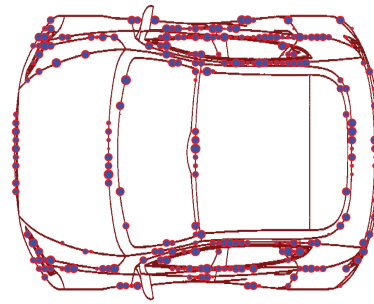

Fig. 12. Extended target model of a car with 273 point scatterers.

comparison results using simulated point targets located at $10°$ and $15°$ are given in Fig. 10, with the same simulation settings used for the other results in this section. The DOA is accurately estimated as $10.2°$ and $15°$ after full compensation with the proposed modified steering vector. This includes the compensation of both the approximation error due to the rounding operation in (13), and the error due to the presence of a velocity component in the cross-forward direction. It can also be seen that compensating for only the former error (denoted by a_{ea}) has a larger impact than compensating for only the latter error (denoted by a_{ev}).

When compensating for the effects of the presence of a cross-forward velocity component, the measurement error in the resulting phase might be significant, especially when operating at mmWave as in automotive radar. To analyze the impact of this velocity component and inaccuracies of this velocity component estimation, velocity measurement errors of different magnitudes have been considered in a Monte Carlo simulation. Their effect on the calculation of the time tag and subsequent compensation of the steering vector is then checked. Specifically, 500 simulations under SNR equal to 20 dB are performed with the radar moving at $10\,\mathrm{m/s}$ in the forward direction-y, and at nominal $2\,\mathrm{m/s}$ in the cross-forward direction-x. The DOA MSE performance as a function of different magnitudes of the measurement error for the compensated velocity is compared in Fig. 11. As expected, not compensating at all with the proposed steering vector yields the highest MSE (plot denoted by "WC"), whereas the ideal compensation, i.e., compensation that has no added velocity measurement error, yields the lowest MSE (plot denoted by "CWT"). Notably, even when there are velocity measurement errors, there is an advantage in applying the proposed compensation based on the modified steering vector, as the resulting MSE is lower than the case of not compensating at all (three plots denoted by "CW"). This shows the advantage of applying the proposed

approach, even in the presence of a measurement error that would prevent reaching the ideal, error-free result.

B. Complex Extended Targets

To demonstrate the imaging capabilities of the proposed method beyond ideal point targets, simulated models of vehicles perceived as extended targets are used. Each car model is represented by 273 point scatterers, which are generated randomly from the edges of the car, as shown in Fig. 12.

In this work, the amplitude of all scatterers is drawn from the uniform distribution, $\alpha_{\mathbf{o}} = \mathcal{U}(0.5, 1)$. According to the Swerling model III [57], during a limited amount of snapshots (essentially one coherent processing interval), the amplitude can be seen as a constant. These scatterers are also assumed to be isotropic and provide constant amplitude and phase of the scattered field during the processing period, as in [58]. The two cars have the same size, with width 2 m and length 4.8 m. According to the traffic rules, the spatial separation between them is 1 m. Both cars are located at a 20 m distance from the radar, and the angle is approximately $0°$ at the broadside. Using (9), we can
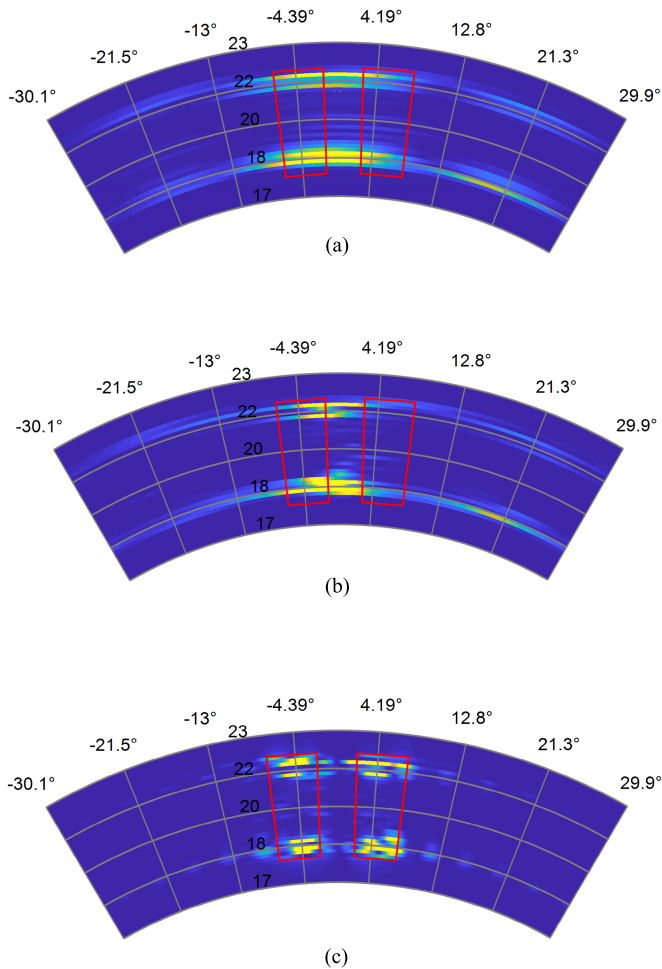
(a)

(b)

(c)

Fig. 13. Simulated performance comparison of extended targets, where the red region is the ground truth of the vehicle. (a) Original beamscan method. (b) IAA-APES method. (c) Proposed method with the expanded aperture size equal to 56.
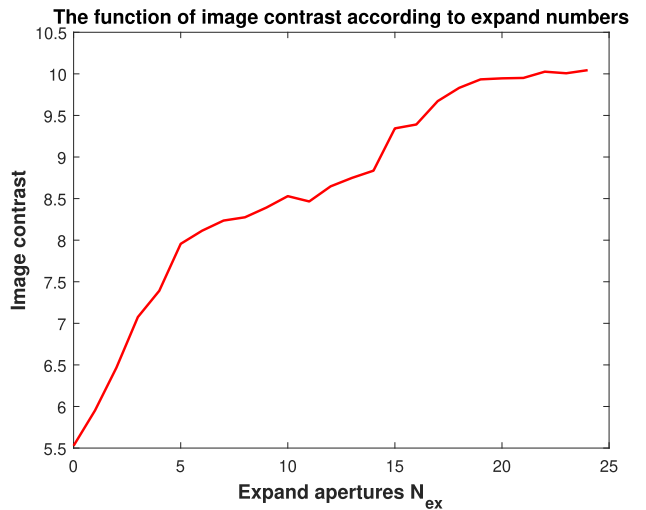

Fig. 14. Image contrast metric as a function of different aperture sizes formed in the proposed method (parameter N_{ex} described in Section III).
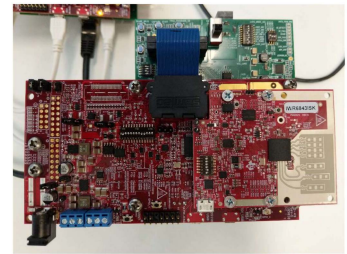

Fig. 15. Radar with the DSP and data capturing boards for experimental verification, where the blue arrow shows the direction of movement.

simulate the dechirped signal for the car's scatterers, which are essentially treated as two extended targets. The results of the range-angle map with different DOA estimation methods are shown in Fig. 13, comparing the proposed method with the traditional beamscan and IAA-APES. As the compressed sensing-based method typically requires knowing the Doppler information of each target a priori, it is not suitable for our extended targets simulation. Empirically, the capability of the proposed method to separate the two extended targets in the angular domain can be seen.

For performance evaluation, because of the relative poor angular resolution, the extended targets cannot be imaged in fine details as done for Lidar or camera systems, which invalidate the usage of performance metrics, such as branching factor, missing factor, and quality percentage [59]. It is also not straightforward to compare the result directly with ground truth, as done for point targets occupying only one single range-angle cell, or in the evaluation of precise range and Doppler estimation methods via the MSE metric [60].

For a quantitative comparison, in this work, the image contrast metric is introduced to demonstrate the separation ability of the proposed method. Image contrast shows the differences in the intensity of each pixel of the image, which is used to evaluate the sidelobe suppression on SAR images [61], [62]. Suppose that the two extended targets are better separated because of the improved angular resolution. In that case, the intensity values in the interval between them will be lower, leading to an increased image contrast value. The image contrast C is defined as

$$C = \frac{\sqrt{E\left\{\left[I^2(i,j) - E\left(I^2(i,j)\right)\right]^2\right\}}}{E\left(I^2(i,j)\right)} \quad (32)$$

where $I^2(i,j)$ is the pixel intensity of (i,j); $E[\bullet]$ is the mean operation. The image contrast is calculated with 50 Monte Carlo repetitions of two car models in different locations within the radar's view. The average results of different scenarios from the range angle map of the cars in the scene for different MSs formed are shown in Fig. 14. It is shown that the higher the number of apertures formed, the higher the value of the image contrast metric, meaning the better the separation capability for the considered extended targets.

C. Experimental Tests and Results

The proposed approach is verified by experimental data. The radar used is the TI IWR6843ISK radar, shown in Fig. 15. The parameters of this radar system are shown in Table. II. Two transmit and four receive antennas are used

TABLE II
Radar Parameters for the Experimental
Verification

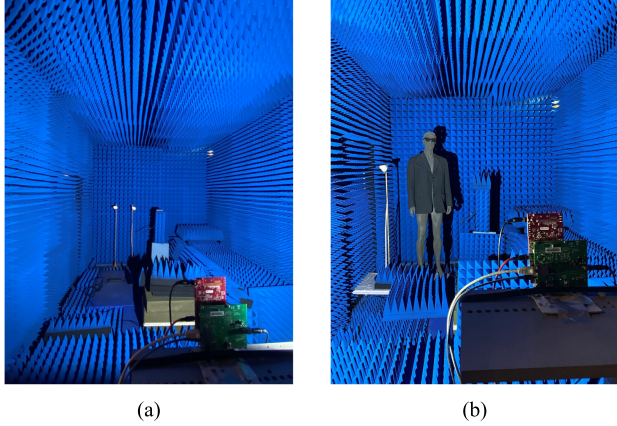| Parameters	Value
Central frequency (GHz)	60
Slope (MHz/μs)	40
Sampling rate (Ms/s)	2.95
Bandwidth (GHz)	3
Number of chirps in snapshot	128
PRI(μs)	100

(a)   (b)

Fig. 16. Experimental scene in the MS3 group's anechoic chamber. (a) With two corner reflectors. (b) With a human model and a corner reflector.

for azimuth angle estimation during the measurement, and the spacing between adjacent receive antennas is half of the wavelength. The radar is installed on a moving platform, and the experimental measurement campaign was performed in the anechoic chamber at TU Delft. The experimental scene is shown in Fig. 16.

Because of the limitations of the moving platform in the chamber, the radar speed is set as $v_y = 0.5$ m/s, which meets the condition in (29). The experimental results for the two corner reflectors and the corresponding control experiment, i.e., the empty chamber, are shown in Fig. 17. With 18 MSs formed in the proposed method, the total number of virtual apertures is equivalent to 26 channels, and the 2 targets can be well separated and their DOA estimated at $-8.9°$ and $-18.5°$. The same results are also shown in Fig. 18 for the human model and corner reflector, which provide the estimation result as $-18.9°$ and $-28.9°$. The control empty chamber line shows no significant artifacts from the method as there are already some minor reflections in the chamber. The control empty chamber angle responses in the two cases are different because the background objects and absorbing materials have been partially moved in order to move the human model without damaging the absorbing materials. Also, the two responses are extracted from different range bins. As shown also in Sections IV-A and IV-B, the larger aperture size is generated, the better angular resolution we can have.

An experiment for the human model and corner reflector with a cross-forward direction velocity of $v_x = 0.1$ m/s was also performed. After compensating the velocity with the
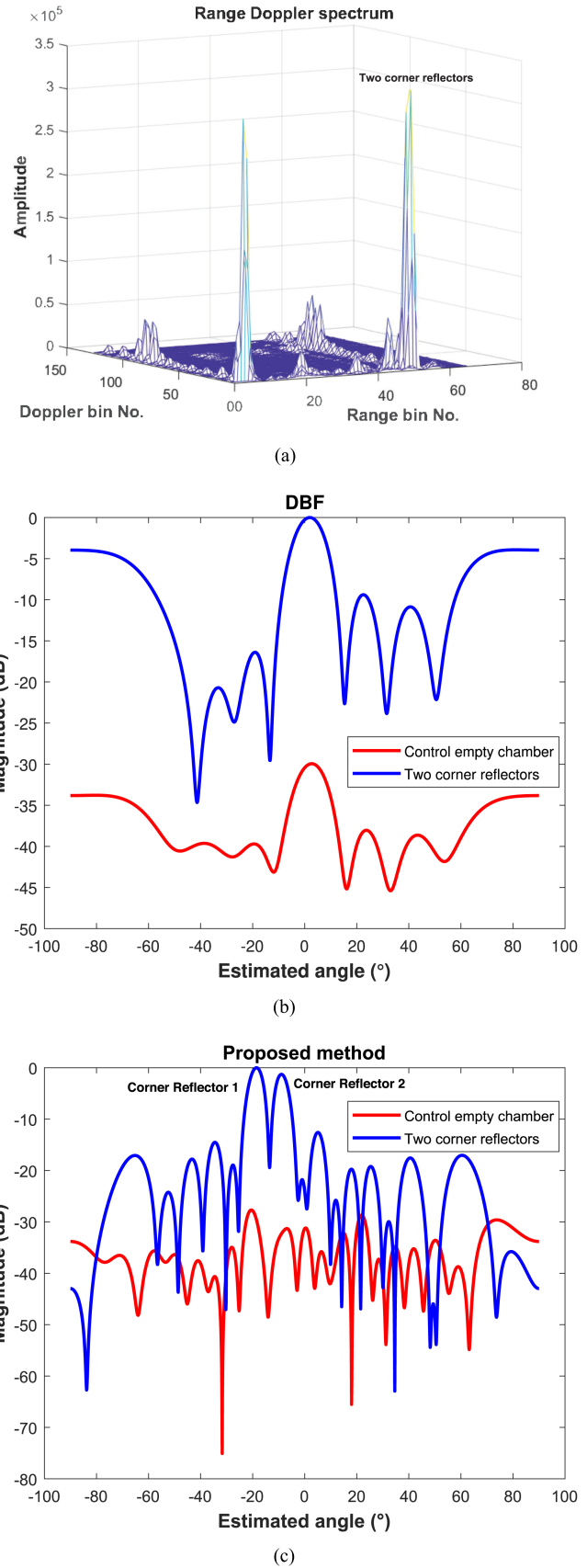

(a)

(b)

(c)

Fig. 17. Experimental results for two corner reflectors. (a) Range Doppler spectrum. (b) DOA curve based on original beamscan method. (c) DOA curve based on the proposed method with expanded aperture size equal to 26.
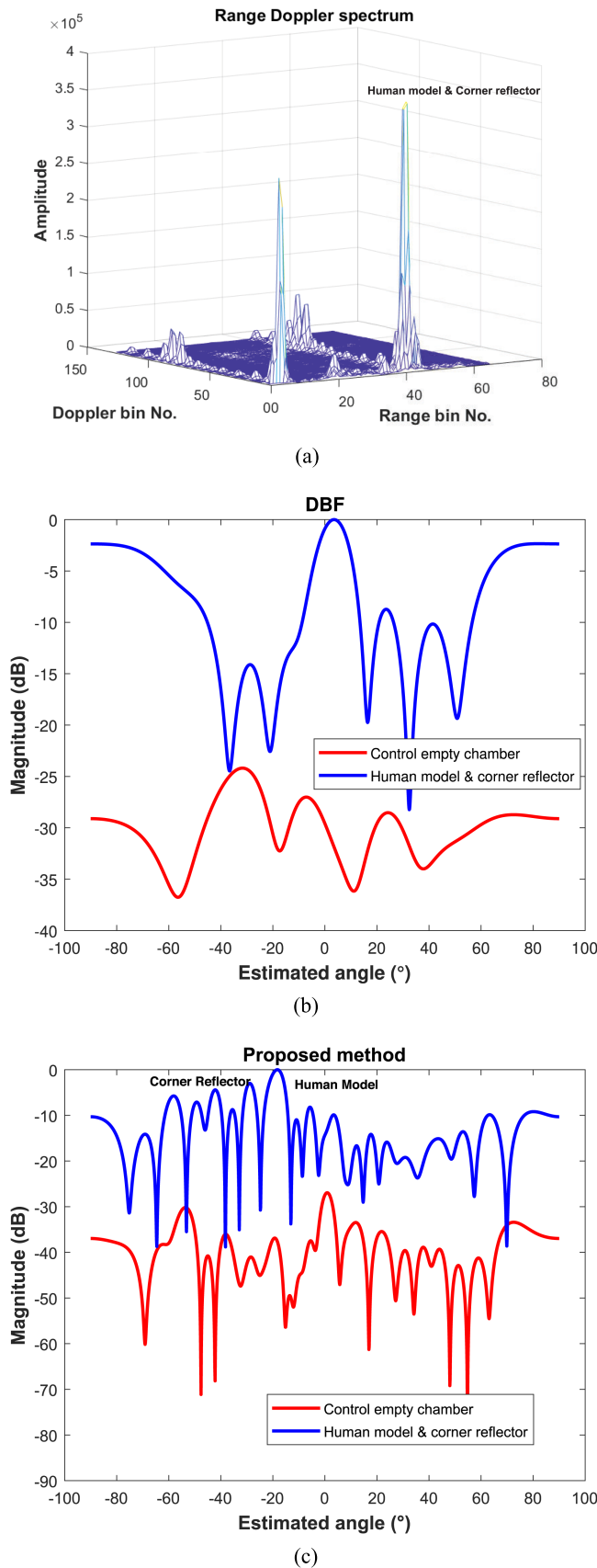
(a)

(b)

Fig. 18. Experimental results for human model and corner reflector.
(a) Range Doppler spectrum. (b) DOA curve based on original beamscan method. (c) DOA curve based on the proposed method with expanded aperture size equal to 26.
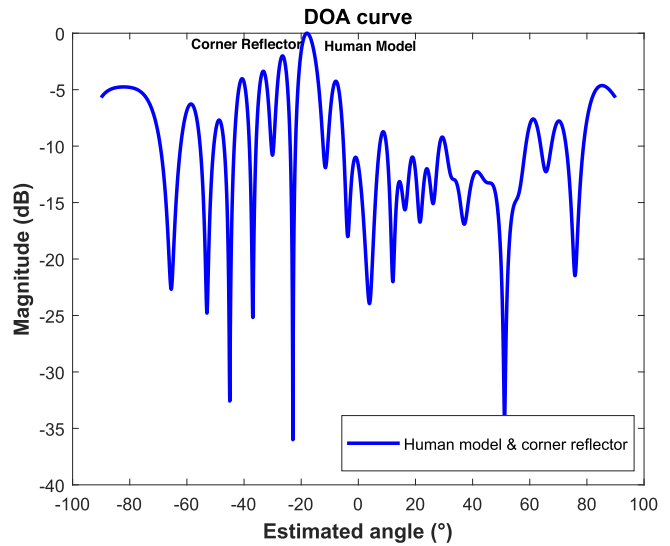

Fig. 19. DOA curve of the human model and corner reflector based on the proposed method with expanded aperture size equal to 26, when the radar is moving in both the two directions.

modified steering vector, the azimuthal profile is shown in Fig. 19. One can observe that the proposed method can also separate the human model and reflector successfully, given the estimation of $-18.0°$ and $-26.5°$, which is the same as the results without cross-forward movement.

V. CONCLUSION

In this article, we have proposed a high-resolution DOA approach using MIMO azimuthal processing in combination with the vehicle motion. Azimuthal resolution improvement of approximately three times in comparison with existing methods has been demonstrated. The targets can be separated and estimated successfully with a limited amount of snapshots, which other existing methods cannot achieve. Considering the motion-enhanced apertures formed, the modified steering vector is also proposed to compensate for the approximation and the transverse velocity errors. The limitation of applicability and tolerance to the velocity error is also investigated.

We verified the proposed method experimentally by performing measurements with pointlike and extended targets using a MIMO radar. A good agreement between the simulation and experimental results is demonstrated. It is worth noting that the proposed approach does not need any prior information about the environment, the number of targets, or their approximate position. The proposed approach is easy to apply in automotive applications due to its low computational time, and it has excellent robustness in varying scenarios.

REFERENCES

[1] I. Bilik, O. Longman, S. Villeval, and J. Tabrikian, "The rise of radar for autonomous vehicles: Signal processing solutions and future research directions," *IEEE Signal Process. Mag.*, vol. 36, no. 5, pp. 20–31, Sep. 2019.

[2] F. Engels, P. Heidenreich, A. M. Zoubir, F. K. Jondral, and M. Wintermantel, "Advances in automotive radar: A framework on computationally efficient high-resolution frequency estimation," *IEEE Signal Process. Mag.*, vol. 34, no. 2, pp. 36–46, Mar. 2017.

[3] R. Feng, F. Uysal, P. Aubry, and A. Yarovoy, "MIMO–monopulse target localisation for automotive radar," *IET Radar, Sonar, Navigation*, vol. 12, no. 10, pp. 1131–1136, 2018.

[4] V. Milanés, S. E. Shladover, J. Spring, C. Nowakowski, H. Kawazoe, and M. Nakamura, "Cooperative adaptive cruise control in real traffic situations," *IEEE Trans. Intell. Transp. Syst.*, vol. 15, no. 1, pp. 296–305, Feb. 2014.

[5] M. Ibarra-Arenado, T. Tjahjadi, J. Pérez-Oria, S. Robla-Gómez, and A. Jiménez-Avello, "Shadow-based vehicle detection in urban traffic," *Sensors*, vol. 17, no. 5, 2017, Art. no. 975.

[6] B. Zhu, S. Yan, J. Zhao, and W. Deng, "Personalized lane-change assistance system with driver behavior identification," *IEEE Trans. Veh. Technol.*, vol. 67, no. 11, pp. 10293–10306, Nov. 2018.

[7] J. Hasch, "Driving towards 2020: Automotive radar technology trends," in *Proc. IEEE MTT-S Int. Conf. Microw. Intell. Mobility*, 2015, pp. 1–4.

[8] S. M. Patole, M. Torlak, D. Wang, and M. Ali, "Automotive radars: A review of signal processing techniques," *IEEE Signal Process. Mag.*, vol. 34, no. 2, pp. 22–35, Mar. 2017.

[9] F. Roos, J. Bechter, C. Knill, B. Schweizer, and C. Waldschmidt, "Radar sensors for autonomous driving: Modulation schemes and interference mitigation," *IEEE Microw. Mag.*, vol. 20, no. 9, pp. 58–72, Sep. 2019.

[10] J. Wang, P. Aubry, and A. Yarovoy, "3-D short-range imaging with irregular MIMO arrays using NUFFT-based range migration algorithm," *IEEE Trans. Geosci. Remote Sens.*, vol. 58, no. 7, pp. 4730–4742, Jul. 2020.

[11] Y. K. Chan and V. C. Koo, "An introduction to synthetic aperture radar (SAR)," *Prog. Electromagn. Res.*, vol. 2, pp. 27–60, 2008.

[12] E. Biglieri, R. Calderbank, A. Constantinides, A. Goldsmith, A. Paulraj, and H. V. Poor, *MIMO Wireless Communications*. Cambridge, U.K.: Cambridge Univ. Press, 2007.

[13] S. Sun, A. P. Petropulu, and H. V. Poor, "MIMO radar for advanced driver-assistance systems and autonomous driving: Advantages and challenges," *IEEE Signal Process. Mag.*, vol. 37, no. 4, pp. 98–117, Jul. 2020. [Online]. Available: https://ieeexplore.ieee.org/document/9127853/

[14] P. Barton, "Digital beam forming for radar," in *Proc. Inst. Elect. Eng. F. (Commun., Radar, Signal Process.)*, vol. 127, pp. 266–277, Aug. 1980.

[15] J. Capon, "High-resolution frequency-wavenumber spectrum analysis," *Proc. IEEE*, vol. 57, no. 8, pp. 1408–1418, Aug. 1969.

[16] S. Xu, J. Wang, and A. Yarovoy, "Super resolution DOA for FMCW automotive radar imaging," in *Proc. IEEE Conf. Antenna Meas. Appl.*, 2018, pp. 1–4.

[17] S. Xu and A. Yarovoy, "Joint Doppler and DOA estimation using 2D MUSIC in presence of phase residual," in *Proc. Eur. Radar Conf.*, 2017, vol. 10, pp. 203–206.

[18] R. Roy and T. Kailath, "ESPRIT-estimation of signal parameters via rotational invariance techniques," *IEEE Trans. Acoust., Speech, Signal Process.*, vol. 37, no. 7, pp. 984–995, Jul. 1989.

[19] Y. Fang, S. Zhu, C. Zeng, Y. Gao, and S. Li, "DOA estimations with limited snapshots based on improved rank-one correlation model in unknown nonuniform noise," *IEEE Trans. Veh. Technol.*, vol. 70, no. 10, pp. 10308–10319, Oct. 2021.

[20] C. Zeng, S. Zhu, S. Li, Q. Liao, and L. Wang, "Sparse frame DOA estimations via a rank-one correlation model for low SNR and limited snapshots," *Appl. Comput. Harmon. Anal.*, vol. 41, no. 2, pp. 362–383, 2016.

[21] T.-J. Shan, M. Wax, and T. Kailath, "On spatial smoothing for direction-of-arrival estimation of coherent signals," *IEEE Trans. Acoust., Speech, Signal Process.*, vol. ASSP-33, no. 4, pp. 806–811, Aug. 1985.

[22] Y. Guercan and A. Yarovoy, "Super-resolution algorithm for joint range-Azimuth-Doppler estimation in automotive radars," in *Proc. Eur. Radar Conf.*, 2017, pp. 73–76.

[23] S. Yuan, F. Fioranelli, and A. Yarovoy, "An approach for high-angular resolution implementation in moving automotive MIMO radar," in *Proc. 18th Eur. Radar Conf.*, 2022, pp. 449–452.

[24] W. Zhang, P. Wang, N. He, and Z. He, "Super resolution DOA based on relative motion for FMCW automotive radar," *IEEE Trans. Veh. Technol.*, vol. 69, no. 8, pp. 8698–8709, Aug. 2020.

[25] X. Gao, S. Roy, and G. Xing, "MIMO-SAR: A hierarchical high-resolution imaging algorithm for FMCW automotive radar," *IEEE Trans. Veh. Technol.*, vol. 70, no. 8, pp. 7322–7334, Aug. 2021, doi: 10.1109/TVT.2021.3092355.

[26] H. Iqbal, A. Löffler, M. N. Mejdoub, D. Zimmermann, and F. Gruson, "Imaging radar for automated driving functions," *Int. J. Microw. Wireless Technol.*, vol. 13, pp. 682–690, 2021.

[27] M. Manzoni et al., "Residual motion compensation in automotive MIMO SAR imaging," in *Proc. IEEE Radar Conf.*, New York City, NY, USA, 2022, pp. 1–7, doi: 10.1109/Radar-Conf2248738.2022.9764310.

[28] S. L. Cassidy, S. Pooni, M. Cherniakov, E. G. Hoare, and M. S. Gashinova, "High resolution automotive imaging using MIMO radar and Doppler beam sharpening," *IEEE Trans. Aerosp. Electron. Syst.*, vol. 59, no. 2, pp. 1495–1505, Apr. 2023.

[29] S. Yuan, P. Aubry, F. Fioranelli, and A. G. Yarovoy, "A novel approach to unambiguous Doppler beam sharpening for forward-looking MIMO radar," *IEEE Sensors J.*, vol. 22, no. 23, pp. 23494–23506, Dec. 2022.

[30] S. Xu, B. J. Kooij, and A. Yarovoy, "Joint Doppler and DOA estimation using (ultra-) wideband FMCW signals," *Signal Process.*, vol. 168, 2020, Art. no. 107259.

[31] S. Xu and A. Yarovoy, "Joint features extraction for multiple moving targets using (ultra-) wideband FMCW signals in the presence of Doppler ambiguity," *IEEE Trans. Signal Process.*, vol. 68, pp. 6562–6577, 2020.

[32] M. L. L. de Oliveira and M. J. Bekooij, "Deep-MLE: Fusion between a neural network and MLE for a single snapshot DOA estimation," in *Proc. IEEE Int. Conf. Acoust., Speech, Signal Process.*, 2022, pp. 3673–3677.

[33] C. Liu, W. Feng, H. Li, and H. Zhu, "Single snapshot DOA estimation based on spatial smoothing music and CNN," in *Proc. IEEE Int. Conf. Signal Process., Commun., Comput.*, 2021, pp. 1–5.

[34] M. L. L. de Oliveira and M. J. Bekooij, "ResNet applied for a single-snapshot DOA estimation," in *Proc. IEEE Radar Conf.*, 2022, pp. 1–6.

[35] I. Roldan, F. Fioranelli, and A. Yarovoy, "Enhancing angular resolution using neural networks in automotive radars," in *Proc. 18th Eur. Radar Conf.*, 2022, pp. 58–61.

[36] P. Hacker and B. Yang, "Single snapshot DOA estimation," *Adv. Radio Sci.*, vol. 8, pp. 251–256, 2010. [Online]. Available: https://ars.copernicus.org/articles/8/251/2010/

[37] W. Liao and A. Fannjiang, "Music for single-snapshot spectral estimation: Stability and super-resolution," *Appl. Comput. Harmon. Anal.*, vol. 40, no. 1, pp. 33–67, 2016.

[38] Y. Ma, Y. Zeng, and S. Sun, "A deep learning based super resolution DOA estimator with single snapshot MIMO radar data," *IEEE Trans. Veh. Technol.*, vol. 71, no. 4, pp. 4142–4155, Apr. 2022.

[39] S. Fortunati, R. Grasso, F. Gini, M. S. Greco, and K. LePage, "Single-snapshot DOA estimation by using compressed sensing," *EURASIP J. Adv. Signal Process.*, vol. 2014, no. 1, pp. 1–17, 2014.

[40] K. Srinivas, S. Ganguly, and P. K. Kumar, "Performance comparison of reconstruction algorithms in compressive sensing based single snapshot DOA estimation," *IETE J. Res.*, vol. 68, pp. 2876–2884, 2020.

[41] W. Roberts, P. Stoica, J. Li, T. Yardibi, and F. A. Sadjadi, "Iterative adaptive approaches to MIMO radar imaging," *IEEE J. Sel. Topics Signal Process.*, vol. 4, no. 1, pp. 5–20, Feb. 2010.

[42] T. Yardibi, J. Li, P. Stoica, M. Xue, and A. B. Baggeroer, "Source localization and sensing: A nonparametric iterative adaptive approach based on weighted least squares," *IEEE Trans. Aerosp. Electron. Syst.*, vol. 46, no. 1, pp. 425–443, Jan. 2010.

[43] W. Wei et al., "DOA estimation of distributed mmWave radar system via fast iterative adaptive approach," in *Proc. Int. Conf. Control, Automat., Inf. Sci.*, 2021, pp. 414–418.

[44] E. Aboutanios, A. Hassanien, M. G. Amin, and A. M. Zoubir, "Fast iterative interpolated beamforming for accurate single-snapshot DOA estimation," *IEEE Geosci. Remote Sens. Lett.*, vol. 14, no. 4, pp. 574–578, Apr. 2017.

[45] F. Roos et al., "Compressed sensing based single snapshot DOA estimation for sparse MIMO radar arrays," in *Proc. 12th German Microw. Conf.*, 2019, pp. 75–78.

[46] R. Cao, B. Liu, F. Gao, and X. Zhang, "A low-complex one-snapshot DOA estimation algorithm with massive ULA," *IEEE Commun. Lett.*, vol. 21, no. 5, pp. 1071–1074, May 2017.

[47] G. Qin, M. G. Amin, and Y. D. Zhang, "DOA estimation exploiting sparse array motions," *IEEE Trans. Signal Process.*, vol. 67, no. 11, pp. 3013–3027, Jun. 2019.

[48] S. Li and X.-P. Zhang, "A new approach to construct virtual array with increased degrees of freedom for moving sparse arrays," *IEEE Signal Process. Lett.*, vol. 27, pp. 805–809, 2020.

[49] D. Johnson and D. Dudgeon, *Array Signal Processing: Concepts and Techniques*. Hoboken, NJ, USA: Prentice-Hall, 1993.

[50] G. Kim, J. Mun, and J. Lee, "A peer-to-peer interference analysis for automotive chirp sequence radars," *IEEE Trans. Veh. Technol.*, vol. 67, no. 9, pp. 8110–8117, Sep. 2018.

[51] A. Angelov, A. Robertson, R. Murray-Smith, and F. Fioranelli, "Practical classification of different moving targets using automotive radar and deep neural networks," *IET Radar, Sonar, Navigation*, vol. 12, no. 10, pp. 1082–1089, 2018.

[52] P. Bokare and A. Maurya, "Acceleration-deceleration behaviour of various vehicle types," *Transp. Res. Procedia*, vol. 25, pp. 4733–4749, 2017. [Online]. Available: https://www.sciencedirect.com/science/article/pii/S2352146517307937

[53] P. Stoica and A. Nehorai, "Music, maximum likelihood, and Cramer-Rao bound," *IEEE Trans. Acoust., Speech, Signal Process.*, vol. 37, no. 5, pp. 720–741, May 1989.

[54] M. Grant and S. Boyd, "Graph implementations for nonsmooth convex programs," in *Recent Advances in Learning and Control* in Series Lecture Notes in Control and Information Sciences, V. Blondel, S. Boyd, and H. Kimura, Eds. Berlin, Germany: Springer, 2008, pp. 95–110, [Online]. Available: https://stanford.edu/boyd/graph_dcp.html

[55] G. A. Tyler and B. J. Thompson, "Fraunhofer holography applied to particle size analysis a reassessment," *Optica Acta: Int. J. Opt.*, vol. 23, no. 9, pp. 685–700, 1976.

[56] S. J. Wright, *Primal-Dual Interior-Point Methods*. New Delhi, India: SIAM, 1997.

[57] P. Swerling, "Probability of detection for fluctuating targets," *IRE Trans. Inf. Theory*, vol. 6, no. 2, pp. 269–308, 1960.

[58] M. Andres, P. Feil, and W. Menzel, "3D-scattering center detection of automotive targets using 77 GHZ UWB radar sensors," in *Proc. 6th Eur. Conf. Antennas Propag.*, 2012, pp. 3690–3693.

[59] T. Hermosilla, L. A. Ruiz, J. A. Recio, and J. Estornell, "Evaluation of automatic building detection approaches combining high resolution images and LiDAR data," *Remote Sens.*, vol. 3, no. 6, pp. 1188–1210, 2011. [Online]. Available: https://www.mdpi.com/2072-4292/3/6/1188

[60] M. Lasserre, S. Bidon, and F. Le Chevalier, "New sparse-promoting prior for the estimation of a radar scene with weak and strong targets," *IEEE Trans. Signal Process.*, vol. 64, no. 17, pp. 4634–4643, Sep. 2016.

[61] S. Yuan, Z. Yu, C. Li, and S. Wang, "A novel SAR sidelobe suppression method based on CNN," *IEEE Geosci. Remote Sens. Lett.*, vol. 18, no. 1, pp. 132–136, Jan. 2021.

[62] F. Berizzi and G. Corsini, "Autofocusing of inverse synthetic aperture radar images using contrast optimization," *IEEE Trans. Aerosp. Electron. Syst.*, vol. 32, no. 3, pp. 1185–1191, Jul. 1996.

Sen Yuan (Graduate Student Member, IEEE) was born in Shanxi, China, in 1998. He received the Bachelor of Engineering degree in electronic information engineering from Beihang University, Beijing, China, in 2017, and the master's degree in the specialty of synthetic aperture radar (SAR) signal processing from Beihang University in 2020 with Prof. C. Li and Prof. Z. Yu. He is currently working toward the Ph.D. degree in microwave sensing signals and systems with the Delft University of Technology, Delft, The Netherlands, a section within the Department of Microelectronics.

He did an Internship with Tsinghua University, Beijing, about navigation with Dr. X. Chen in 2016. During his graduate education, he studied and became familiar with the SAR, including its satellite orbits, system design, and ground processing. In January 2021, he joined TU Delft. He works on millimeter radar signal processing in automotive applications.

Francesco Fioranelli (Senior Member, IEEE) received the Laurea (B.Eng., *cum laude*) and Laurea Specialistica (M.Eng., *cum laude*) degrees in telecommunication engineering from the Università Politecnica delle Marche, Ancona, Italy, in 2007 and 2010, respectively, and the Ph.D. degree in electronic engineering from Durham University, Durham, U.K., in 2014.

From 2014 to 2016, he was a Research Associate with the University College London, London, U.K., and was an Assistant Professor with the University of Glasgow, Glasgow, U.K., from 2016 to 2019. He is currently an Associate Professor with TU Delft, Delft, The Netherlands. His research interests include the development of radar systems and automatic classification for human signatures analysis in healthcare and security, drones and UAVs detection and classification, automotive radar, wind farm, and sea clutter. He has authored more than 140 publications between book chapters, journal and conference papers, edited the books "Micro-Doppler Radar and Its Applications" and "Radar Countermeasures for Unmanned Aerial Vehicles" published by IET-Scitech in 2020.

Dr. Fioranelli is a recipient of three best paper awards.

Alexander G. Yarovoy (Fellow, IEEE) received the Diploma (with Hons.) in radiophysics and electronics and the Candidate Phys. & Math. Sci. and Doctor Phys. & Math. Sci. degrees in radiophysics from Kharkov State University, Kharkiv, Ukraine, in 1984, 1987, and 1994, respectively.

In 1987, he joined the Department of Radiophysics, Kharkov State University, as a Researcher, and became a Full Professor there in 1997. From 1994 to 1996, he was at the Technical University of Ilmenau, Germany, as a Visiting Researcher. Since 1999, he has been with the Delft University of Technology, Delft, The Netherlands. Since 2009, he has been leading there as a Chair of Microwave Sensing, Systems and Signals. He has authored and coauthored more than 500 scientific or technical papers, 7 patents, and 14 book chapters. His main research interests include high-resolution radar, microwave imaging, and applied electromagnetics (in particular, UWB antennas).

Dr. Yarovoy is the recipient of the European Microwave Week Radar Award for the paper that best advances the state of the art in radar technology in 2001 (together with L. P. Ligthart and P. van Genderen) and in 2012 (together with T. Savelyev). In 2010, together with D. Caratelli, he got the best paper award of the Applied Computational Electromagnetic Society. He was the General TPC Chair of the 2020 European Microwave Week, the Chair and the TPC Chair of the 5th European Radar Conference, as well as the Secretary of the 1st European Radar Conference. He was also the Co-Chair and the TPC Chair of the Xth International Conference on GPR. He is also an Associate Editor for IEEE TRANSACTION ON RADAR SYSTEMS. From 2011 to 2018, he was an Associate Editor for the *International Journal of Microwave and Wireless Technologies*. From 2008 to 2017, he was the Director of the European Microwave Association.